Chemical and Process Engineering 2014, 35 (3), 293-304
DOI: 10.2478/cpe-2014-0022

CFD ANALYSIS OF HEAT TRANSFER IN A MICROTUBULAR SOLID OXIDE FUEL CELL STACK

Paulina Pianko-Oprych*, Ekaterina Kasilova, Zdzisław Jaworski

West Pomeranian University of Technology, Institute of Chemical Engineering and Environmental Protection Processes, al. Piastów 42, 71-065 Szczecin, Poland

The aim of this work was to achieve a deeper understanding of the heat transfer in a microtubular Solid Oxide Fuel Cell (mSOFC) stack based on the results obtained by means of a Computational Fluid Dynamics tool. Stack performance predictions were based on simulations for a 16 anode-supported mSOFCs sub-stack, which was a component of the overall stack containing 64 fuel cells. The emphasis of the paper was put on steady-state modelling, which enabled identification of heat transfer between the fuel cells and air flow cooling the stack and estimation of the influence of stack heat losses. Analysis of processes for different heat losses and the impact of the mSOFC reaction heat flux profile on the temperature distribution in the mSOFC stack were carried out. Both radiative and convective heat transfer were taken into account in the analysis. Two different levels of the inlet air velocity and three different values of the heat losses were considered. Good agreement of the CFD model results with experimental data allowed to predict the operation trends, which will be a reliable tool for optimisation of the working setup and ensure sufficient cooling of the mSOFC stack.

Keywords: microtubular Solid Oxide Fuel Cell stack, heat transfer, heat losses, temperature distributions, Computational Fluid Dynamics

1. INTRODUCTION

Understanding the mechanisms of heat transfer in a microtubular Solid Oxide Fuel Cell (mSOFC) stack is of key importance for improving heat management of the system. Energy is transported in the stack through the stack channels being accompanied by mass flow and chemical reactions. Reactants diffuse into the cell walls to participate in electrochemical reactions and release energy. The Gibbs free energy is partially converted into electrical energy and its portion is released as the reaction heat. A part of the electrical energy is supplied to the external load and the other part is consumed by the intrinsic resistance and then is converted to heat. Due to temperature differences in the stack, the cell walls exchange heat with fuel and cathode air. Temperatures of the fuel and air affect the heat transfer processes and the temperature of the cell (Huang et al., 2013). Thus heat transfer processes occur simultaneously to the mass and momentum transfer processes and chemical reactions. The reactant partial pressures and the temperature affect the voltage output that the mSOFC stack can produce. On the one hand, the external load determines the current that the mSOFC stack produces and the consumption rates of the reactants by the electrochemical reaction, while on the other hand the voltage output is affected by the partial pressures of each species and their temperatures, which in turn affect the heat exchange process inside the mSOFC stack and the fuel cell temperatures. Useful tools in predictions of the flow of reactants and heat transfer in the mSOFC stack are numerical codes of

*Corresponding author, e-mail: paulina.pianko@zut.edu.pl

Computational Fluid Dynamics (CFD). Other available approaches of mathematical modelling have been presented by Milewski et al. (2011). The authors divided models into two main groups: the classic black box approach, which is based on empirical models with discrete time sampling and the so called white box models or physical modelling based on a very complicated mathematical description.

Understanding the mechanisms of heat transfer in a microtubular Solid Oxide Fuel Cell (mSOFC) stack is of key importance for improving heat management of the system. Energy is transported in the stack through the stack channels being accompanied by mass flow and chemical reactions. Reactants diffuse into the cell walls to participate in electrochemical reactions and release energy. The Gibbs free energy is partially converted into electrical energy and its portion is released as the reaction heat. A part of the electrical energy is supplied to the external load and the other part is consumed by the intrinsic resistance and then is converted to heat. Due to temperature differences in the stack, the cell walls exchange heat with fuel and cathode air. Temperatures of the fuel and air affect the heat transfer processes and the temperature of the cell (Huang et al., 2013). Thus heat transfer processes occur simultaneously to the mass and momentum transfer processes and chemical reactions. The reactant partial pressures and the temperature affect the voltage output that the mSOFC stack can produce. On the one hand, the external load determines the current that the mSOFC stack produces and the consumption rates of the reactants by the electrochemical reaction, while on the other hand the voltage output is affected by the partial pressures of each species and their temperatures, which in turn affect the heat exchange process inside the mSOFC stack and the fuel cell temperatures. Useful tools in predictions of the flow of reactants and heat transfer in the mSOFC stack are numerical codes of Computational Fluid Dynamics (CFD). Other available approaches of mathematical modelling have been presented by Milewski et al. (2011). The authors divided models into two main groups: the classic black box approach, which is based on empirical models with discrete time sampling and the so called white box models or physical modelling based on a very complicated mathematical description.

More recently, Akhtar et al. (2010) and Akhtar (2012) have published numerous reviews of fuel cells modelling dealing with transport phenomena, electrochemical processes and heat management within a single microtubular chamber Solid Oxide Fuel Cell. This 2-dimensional model consider the following methane processing: full combustion, steam reforming, dry reforming and water gas shift reaction followed by electrochemical oxidation of the produced hydrogen within the anode zone. The microtubular single chamber SOFC stack consisted of three fuel cells. The operating cell voltage was set to 0.5 V at the operating temperature of 700^{o}C and the inlet flow velocity of 0.03 m/s. The simulations were performed using the commercial CFD code COMSOL Multiphysics 3.5a. Numerical results allowed for a systematic analysis of a range of parameters, such as porous material filled gas chamber with different values of thermal conductivity and a bare gas chamber without any porous insert on the temperature distribution along the fuel cell length. Akhtar (2012) stated that the gas chamber with the porous material helped in lowering the thermal stresses induced in the fuel cell.

The importance of the coupling between the physical parameters and phenomena within fuel cells was emphasised by Andersson et al. (2012). A fully coupled CFD model was developed in COMSOL Multiphysics to describe an intermediate temperature single cell anode-supported SOFC. The model included governing equations for mass, momentum, heat and charge transport as well as kinetics and considered the internal reforming and electrochemical reactions. The impact on the operating temperature and the cooling effect by the surplus of air flow was investigated. The difference between the inlet and outlet temperatures at constant fuel and air flow rates was varied in the range of 35 - 50^{o}C depending on the change of the fuel and air utilisations (Andersson et al., 2012). A higher temperature within the fuel cell meant a faster consumption of methane and a higher production of carbon monoxide. Thus, a higher temperature gradient decreased the life time of the fuel cell material. It was concluded that CFD simulations were still necessary to fully understand the physical phenomena within the SOFC stack.

Recently, a detailed model that took into account mass, momentum, heat and electric charge transfer was developed for a microtubular SOFC by Amiri et al. (2013). The gas velocity profile, convective and conductive heat and mass transfer were modelled within two porous electrodes and a gas channel. It was found that local heating within the electrode was negligible when the temperature of the middle of the electrode surface was kept constant. Temperature gradients along the cell's active length were found to be non-negligible. However, Amiri et al. (2013) made an important observation that for the particular setup and conditions of the considered system an isothermal model predicted the cell overall performance quite accurately compared to the complete non-isothermal model. This observation is significant from the computational point of view for conducting further optimisation investigations for the mSOFC since solving the isothermal model for each I-V point takes only few minutes to converge to a solution compared to several hours needed for non-isothermal simulations. Nevertheless that assumption can be valid only for a very particular setup and conditions of the system modelled.

It follows from the literature review that efforts to predict temperature distributions in the SOFC have already been reported for many numerical investigations (e.g. Amiri et al. 2013; Andersson et al., 2012; Meier et al., 2012), but still a systematic analysis of a range of effects on the heat transfer processes in the microtubular Solid Oxide Fuel Cell stack is needed for improving the fuel cell heat flux distribution. In this present paper, the influence of heat losses on the temperature distributions in a microtubular Solid Oxide Fuel Cell stack was evaluated. Moreover, the impact of the electrochemically driven heat flux profile on temperature distributions in the mSOFC stack was also analysed.

2. THE METHOD OF MODELLING

The paper was focused on analysing heat transfer of the whole Solid Oxide Fuel Cells stack. The stack contained 64 microtubular SOFC's arranged as an in-line tube bundle. The outer diameter of the fuel cell tubes was 6.7 mm, while the active and the inert lengths of fuel cells were equal to 100.5 mm and 45 mm, respectively (Figure 1).

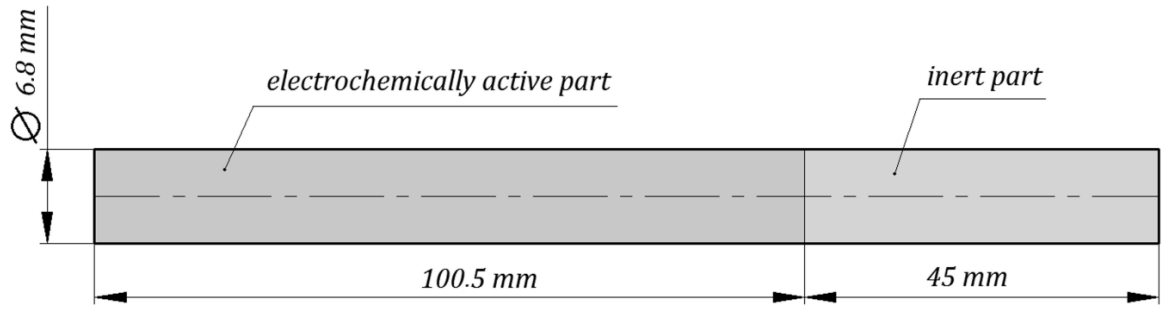

Fig. 1. Geometry of a single microtubular SOFC

According to the published CFD results for mSOFCs (Andersson et al., 2012; Meier et al., 2012) the heat carried away with the fuel flow was much lower than the heat transferred to the cathode air stream. Thus, it was assumed that the fuel cells were cooled mainly by the cathode air flow. Based on that conclusion, it was assumed that temperature distribution in the mSOFC stack was defined by heat transfer between the cell and air flowing in the stack. Therefore, the air volume only was assumed as the computational domain. The effect of the whole group of the processes in the ceramic SOFC electrodes-electrolyte assembly was treated as a reaction of heat flux applied to a boundary of the active SOFC surface with the air volume. The boundary of the inert SOFC surface with the air volume was assumed to be adiabatic.

Heat transfer investigations included two approaches for distribution of the heat flux applied to the active surface of the tubes and analysis of influence of heat losses through walls of the stack.

The CFD model was based on the mass, momentum and energy conservation equations, which were numerically solved in the laminar flow regime and for the steady - state conditions:

$$\nabla \cdot (\rho \bar{u}) = 0 \tag{1}$$

$$\rho(\bar{u} \cdot \nabla)\bar{u} = \nabla \cdot \left(\mu \left[\left(\nabla \bar{u} + \nabla \bar{u}^T \right) - \frac{2}{3} \nabla \cdot \bar{u} I \right] \right) + \rho \bar{g} - \nabla p \tag{2}$$

$$\nabla \cdot (\rho c_p T \bar{u}) = \nabla \cdot (\lambda \nabla T) \tag{3}$$

Emission, absorption and reflection of radiation by solid boundary surfaces of the stack and cell tubes were taking into account using the energy balance for the kth surface:

$$q_{out,k} = \varepsilon_k \sigma T_k^4 + (1 - \varepsilon_k) q_{in,k} \tag{4}$$

where: $q_{out,k}$ is the energy flux leaving the kth surface, ε_k is surface emissivity, σ is the Boltzmann constant, $q_{in,k}$ is the energy flux incident on the surface from surroundings which was calculated as

$$q_{in,k} = \sum_{j=1}^{N} F_{kj} q_{out,j} \tag{5}$$

The cathode air flow was treated as radiatively non-participating media.

Equations (1)-(5) were solved using the commercial CFD software ANSYS Fluent 14.0. The Gambit 2.0 pre-processor was employed to create a 3D geometry of a quarter of the mSOFC stack to reflect the stack symmetry and to build a numerical grid with 89 088 computational cells. The quality of the grid was examined by means of the EquiAngleSkew parameter as well as other grid parameters. The minimum orthogonal quality was 0.88, while the maximum aspect ratio was equal to 2.5. The geometry of the quarter of the mSOFC stack with the numerical mesh is shown in Figure 2.

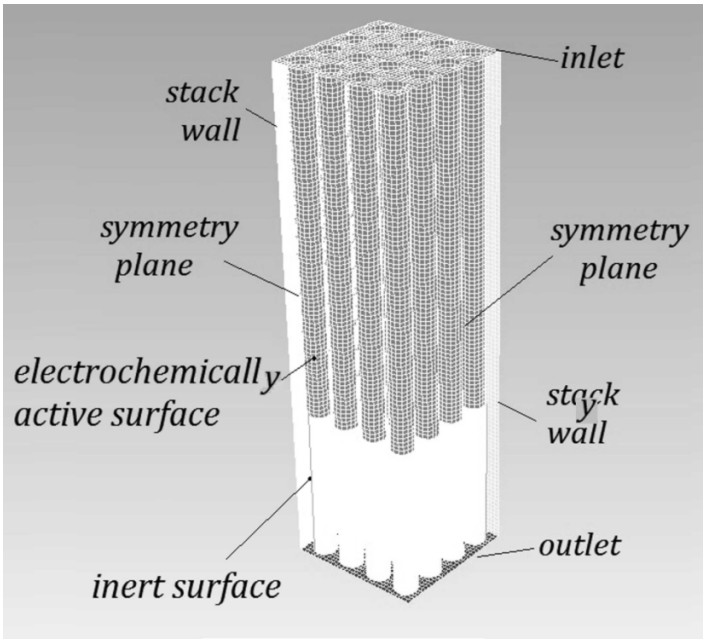

Fig. 2. mSOFC sub-stack arrangement with the numerical mesh

Approach 1. Uniform distribution of the mSOFC reaction heat flux

In the first stage of investigations, uniform distribution of heat flux was assumed on the active surface of the cells. The constant heat flux value, q, was calculated from Equation (6) using an analytical estimation based on experimental I-U curves (Howe et al., 2011):

$$q = \frac{1-\eta}{\eta} \cdot P_{el} \tag{6}$$

where the electrical power density, P_{el}, of 0.3 – 0.5 Wcm^{-2} was the applied range of the power densities, while the mSOFC electrical efficiency, η, equalled to 30-40% was assumed as a pessimistic estimation for the mSOFC electrical efficiency according to the literature data (Howe et al., 2011). The assumed value of the mSOFC electrical efficiency corresponded to 0.4 – 0.5 V of the working voltage. The mSOFC reaction heat flux was assumed a little higher, at 7500 Wm^{-2} for the active fuel cells part in the mSOFC stack simulation and for the ideal case (Case 1) without any heat losses through the stack walls. In the numerical investigations of the two approaches three other values of the stack heat losses were considered and compared with Case 1. In Case 2 the total stack heat losses were close to 5% (375 Wm^{-2}) of the heat power released by the SOFC operation; in Case 3 the heat losses approached 10% (750 Wm^{-2}) of the SOFC reaction heat flux, while in Case 4 they were around 50% (3750 Wm^{-2}) of the SOFC reaction heat flux. The air temperature at the inlet was assumed at 973 K and two levels of the cathode air velocity of 2.0 and 8.5 ms^{-1} were chosen. The outlet surface was set as a pressure outlet. The stack external walls were defined as stationary walls with either zero heat losses for the ideal Case 1 or with non-zero values for Cases 2-4. The inert (anodic) part of the fuel cell tubes was assumed adiabatic. The coupling of heat transfer with electrochemistry and charge transfer was neglected for Case 1, while in Cases 2-4 the SOFC reaction heat flux profile was estimated from literature data and was implemented in the boundary conditions of the active tube surface. The power density of 7500 Wm^{-2} for the generated SOFC reaction heat flux was assumed as a very pessimistic estimation.

Approach 2. Influence of electrochemically-driven non-uniformities of the SOFC reaction heat flux

In the second stage of investigation, the SOFC reaction heat flux profile *q(z)* for the microtubular SOFC with ideal current collectors was expressed by a linear dependence (Equation 7):

$$q = q_{max} - a \cdot q_{mean} \cdot z \tag{7}$$

where a was expressed by Equation (8) in the range of 5 - 15 m^{-1} according to the reference data (Cui et al., 2007; Cui and Cheng, 2009; Doraswami et al., 2010):

$$a = \left(\frac{1}{q_{mean}}\right)\left(\frac{dq}{dz}\right) \tag{8}$$

The value q_{mean} was the surface-averaged value of the SOFC reaction heat flux. Two kinds of the heat flux profile were considered:

$$q(z) = 9.38 \cdot 10^{3} - 3.75 \cdot 10^{4} \cdot z \tag{9}$$

and

$$q(z) = 1.13 \cdot 10^{4} - 7.5 \cdot 10^{4} \cdot z \tag{10}$$

The two reaction heat flux profiles of Approach 2 were included in the mSOFC stack model using Fluent User Defined Function (UDF).

The gas properties based on the ANSYS database were used in the simulations and air was treated as the ideal gas. All the boundary conditions for heat transfer were defined in the ANSYS code. The calculations were performed with the default numerical parameters available in the code unless residuals were stabilised and constant calculation results were achieved. Usually, the normalised residual sum reached the magnitude of 10^{-13} - 10^{-17} at the end of calculations. The converged simulations provided local values of the velocity, pressure and temperature.

The emissivity of the active part of the fuel cell tubes was an unknown parameter. Therefore, a numerical study on the influence of cathode emissivity, $\varepsilon_{cathode,}$ on the mSOFC temperature distribution was also performed. The analysis included consideration of eight values of the cathode emissivity in the range from 0.3 to 1.0 with 0.1 increments. The mSOFC temperature was almost constant along the fuel cell length except at its end. At the end of the fuel cells a temperature drop was observed. Further, temperature drop was stronger for a higher value of the cathode emissivity, e.g. $\varepsilon_{cathode}$=1.0 gave T=977 K, while for $\varepsilon_{cathode}$=0.4 the temperature was equal to T=1040 K. It was concluded that there is a strong influence of cathode emissivity on the mSOFC temperature. The air temperature near the mSOFC walls was closest to the experimental value of 750 ^{o}C (Howe et al., 2013) for the cathode emissivity equal to 0.4.

3. RESULTS AND DISCUSSION

The buoyancy effect similar to natural convection was found to be negligible, while the radiative heat transfer was quite important for the mSOFC cooling. The impact of the radiative heat transfer was estimated close to 20 - 30% of the mSOFC reaction heat flux using the standard surface – to – surface model. The cathode air was regarded as a non-participating media in radiation. The CFD procedure was validated based on the test data of single microtubular SOFC (Morata et al., 2014) due to sparsity of experimental data available for the whole stack. The SOFC temperature obtained by the CFD simulation was varied in the range of 744-753^{o}C. This result matches the corresponding experimental estimation of 720-750 ^{o}C (Howe et al., 2013).

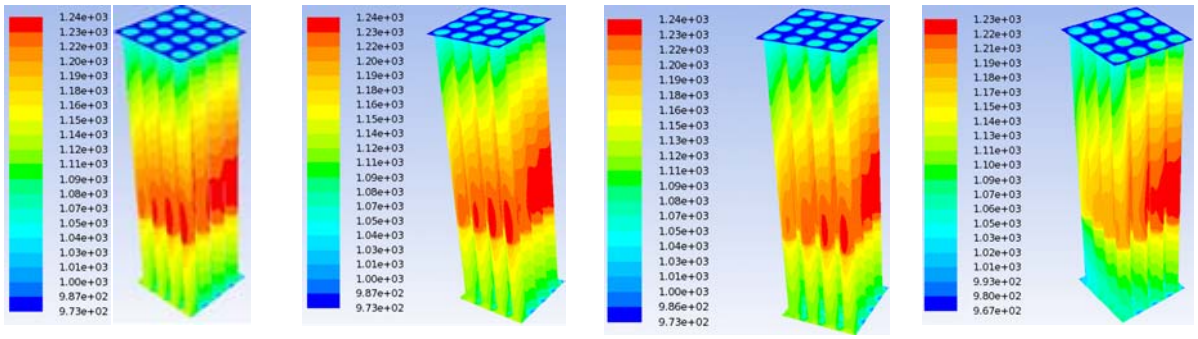

(Case 1) 0% heat losses | (Case 2) 5% heat losses | (Case 3) 10% heat losses | (Case 4) 50% heat losses

Fig. 3. Temperature distribution of the fuel cell tubes at the air inlet velocity of 2.0 ms^{-1} and for different stack heat losses' values of: 0% (Case 1), 5% (Case 2), 10% (Case 3), 50% (Case 4)

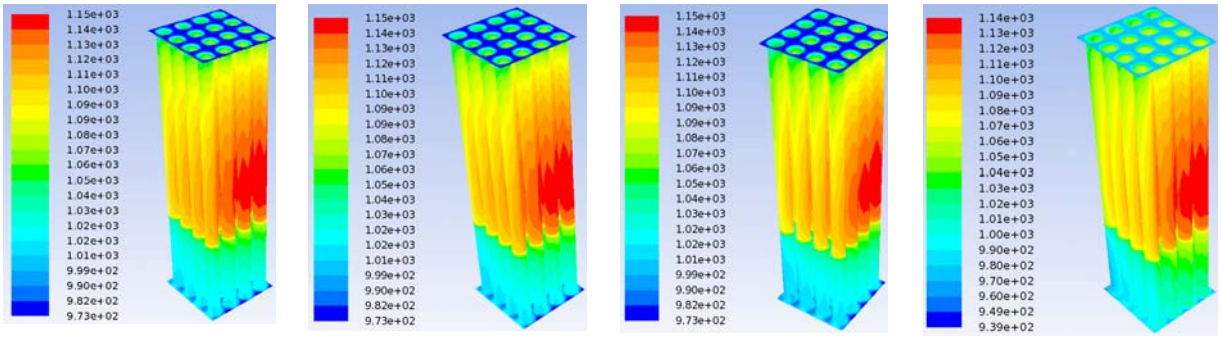

(Case 1) 0% heat losses | (Case 2) 5% heat losses | (Case 3) 10% heat losses | (Case 4) 50% heat losses

Fig. 4. Temperature distribution of the fuel cell tubes at the air inlet velocity of 8.5 ms^{-1} and for different stack heat losses' values of: 0% (Case 1), 5% (Case 2), 10% (Case 3), 50% (Case 4)

In the first numerical approach (Approach 1), temperature distributions in the mSOFC for different percentage values of the reaction heat flux (heat losses): 5, 10 and 50% (Cases 2-4) were compared with the ideal case without heat losses (Case 1) and are shown in Figures 3-4, respectively for 2.0 and 8.5 ms^{-1} of the air velocity.

The simulation results shown in Figures (3, 4) revealed that until stack losses heat flux is up to 5 – 10% of the mSOFC reaction heat flux, the stack losses have a very low impact on the stack thermal conditions. However, the influence of the stack heat losses significantly increases with decreasing air flow velocity for heat losses of 50%.

The stack heat losses increase the temperature gradients across the mSOFC stack as can be seen in Figures 5-6. The stack walls and the external fuel cell tubes became significantly colder, while the middle fuel cell tubes did not reflect the drop of their wall temperature. It means the middle tubes were influenced only by a few adjacent tubes.

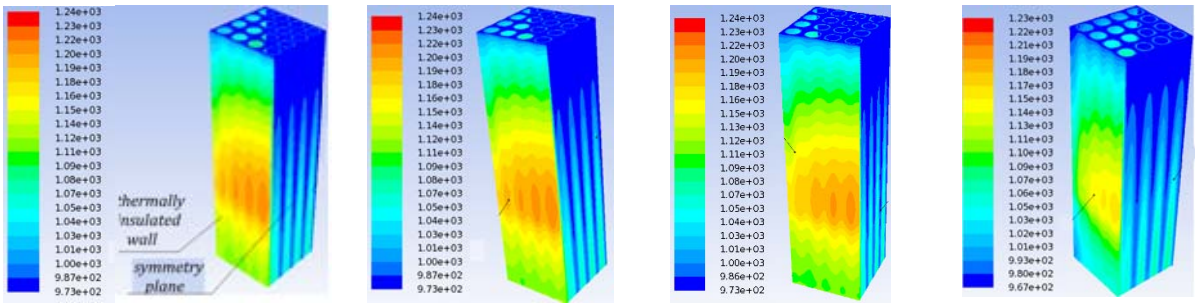

Fig. 5. Temperature distribution on the mSOFC stack walls and symmetry planes at the air inlet velocity of 2.0 ms^{-1} and for different stack heat losses' values of: 0% (Case 1), 5% (Case 2), 10% (Case 3), 50% (Case 4)

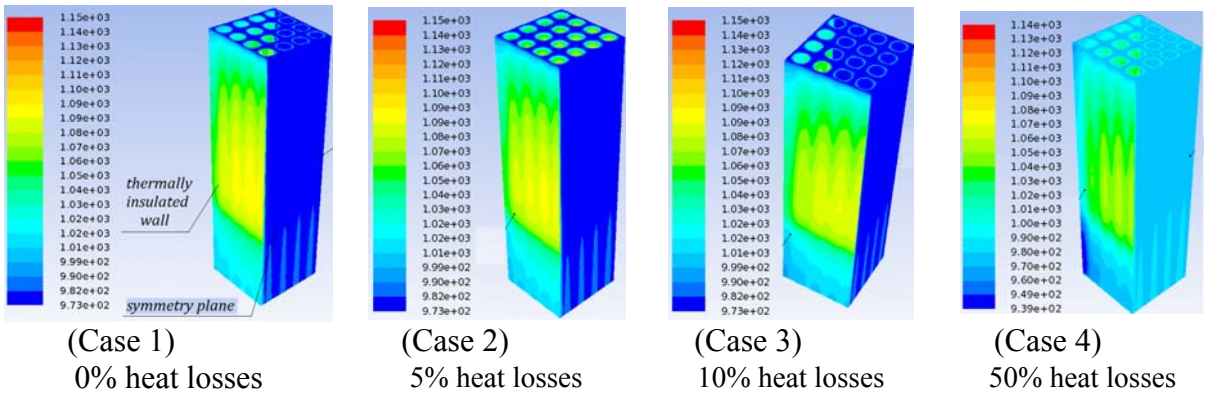

Fig. 6. Temperature distribution on the mSOFC stack walls and symmetry planes at the air inlet velocity of 8.5 ms^{-1} and for different stack heat losses' values of: 0% (Case 1), 5% (Case 2), 10% (Case 3), 50% (Case 4)

Another analysed quantity was the maximum temperature difference between the middle fuel cell tube and the corner one which together with the temperatures of the SOFC tube ends are presented in Figure 7.

The thermal performance of the middle and corner fuel cells obtained from the CFD solutions for the mSOFC stack is presented in Figures 8 – 9. The shape of the temperature distribution curves along the corner and middle fuel cell tubes for the air flow velocity of 2.0 ms^{-1} (Fig. 8) and 8.5 ms^{-1} (Fig. 9) were generally similar. However, much higher temperature rises were observed at the lower value of the air flow velocity. From the temperature comparison between the middle fuel cell tube and the corner one (Figures 8 and 9) it follows that the maximum temperature difference between the corner tube and the

middle one was about 50°C for the two considered air velocity values and at 0, 5 and 10% of heat losses, while for 50% of heat losses the maximum temperature difference between the corner and the middle tubes was significantly higher. Thus, heat losses increase temperature gradients in the stack cross-sections. Similarly, increase of the air flow rate reduces the temperature gradients along the stack: for the highest value of heat losses of 50% the temperature difference between the corner and the middle tubes decreased from 80°C to 30°C while increasing the air flow velocity from 2.0 to 8.5 ms^{-1}.

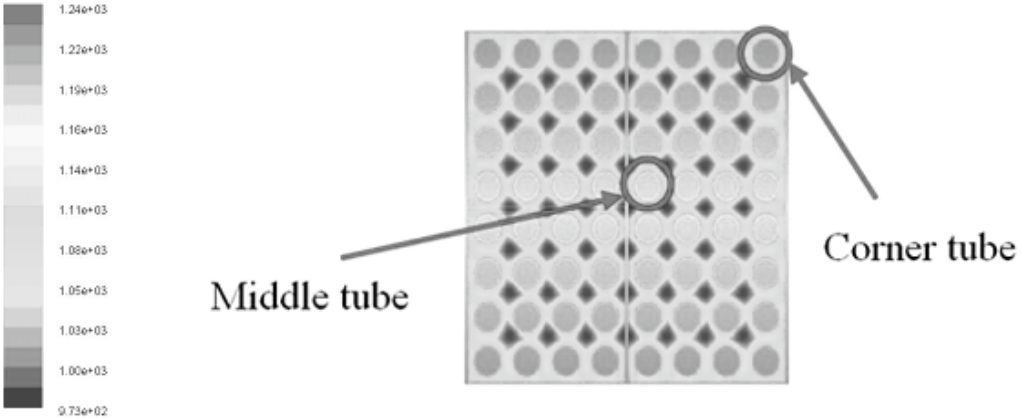

Fig. 7. Fuel cell tubes arrangements in the mSOFC stack and temperature fuel in the outlet cross-section

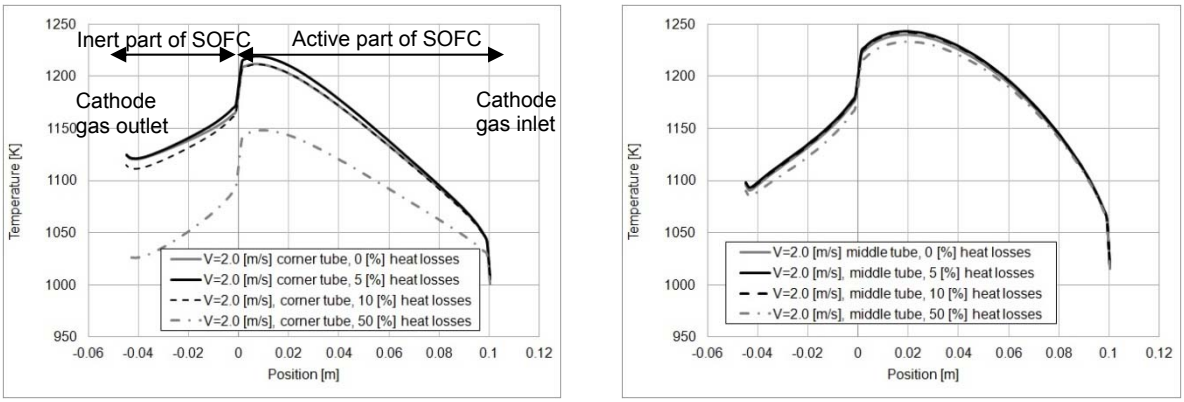

(a) (b)

Fig. 8. Temperature distributions at the air flow velocity of 2.0 ms^{-1} along a corner (a) and middle (b) fuel cell tubes at different stack heat losses' values of: 0, 5, 10 and 50%

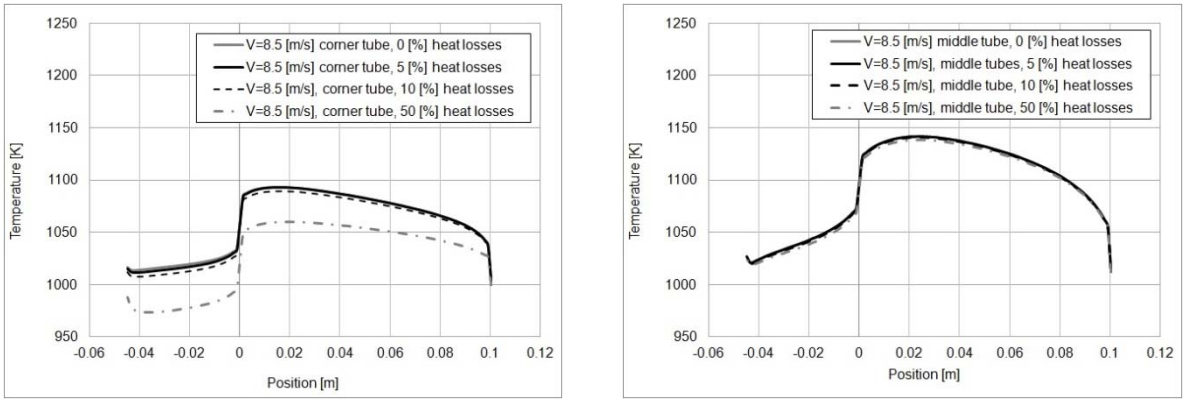

(a) (b)

Fig. 9. Temperature distributions at the air flow velocity of 8.5 ms^{-1} along a corner (a) and middle (b) fuel cell tubes at different stack heat losses' values of: 0, 5, 10 and 50 %

In the second approach (Approach 2), the impact of the electrochemically driven SOFC reaction heat flux profile on temperature distributions in the mSOFC stack was analysed. The results for the mSOFC stack temperature are visually presented in Figures 10 and 11.

At the chosen flow rates the electrochemically driven non-uniformities slightly increase the maximum temperature of the mSOFC and made the temperature distribution along the fuel cell a little steeper.

The highest mSOFC temperature was obtained for the linear heat flux profile at the shape parameter equal to 10 m^{-1}. The temperature of the hottest point on the SOFC surface increased and shifted to the stack inlet-cross-section compared to the case with the uniform heat flux (cf. Figs. 8b and 9b with Fig. 12).

It may be deduced from the CFD results described above that the presented model predicted well temperature distributions for the entire mSOFC stack and the predictions were found to be qualitatively consistent with the literature and experimental results.

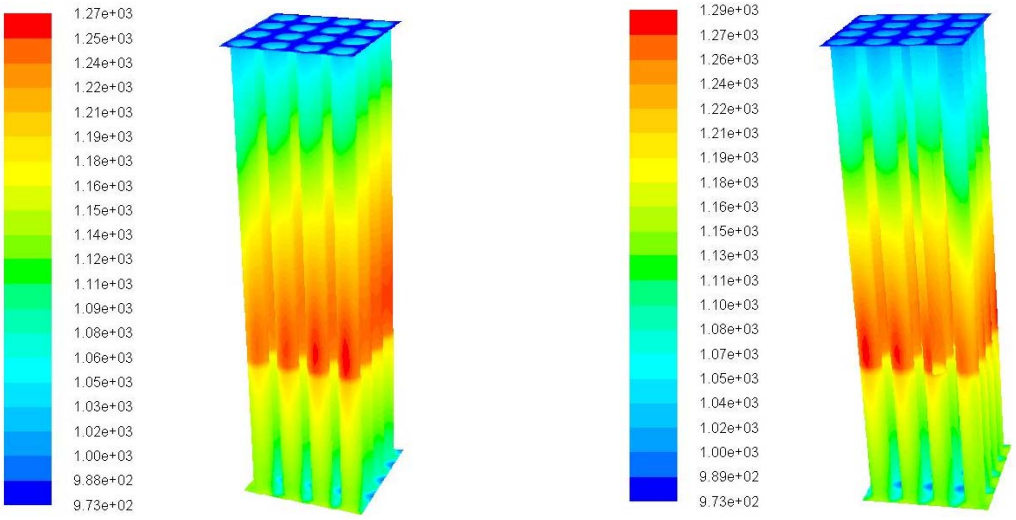

(a) (b)

Fig. 10. Temperature distributions of the fuel cell tubes at the air inlet velocity of 2.0 ms^{-1} with 7500 Wm^{-2} stack heat losses for two shape parameters of the linear SOFC heat flux profile: (a) a = 5 m^{-1} and (b) a = 10 m^{-1}

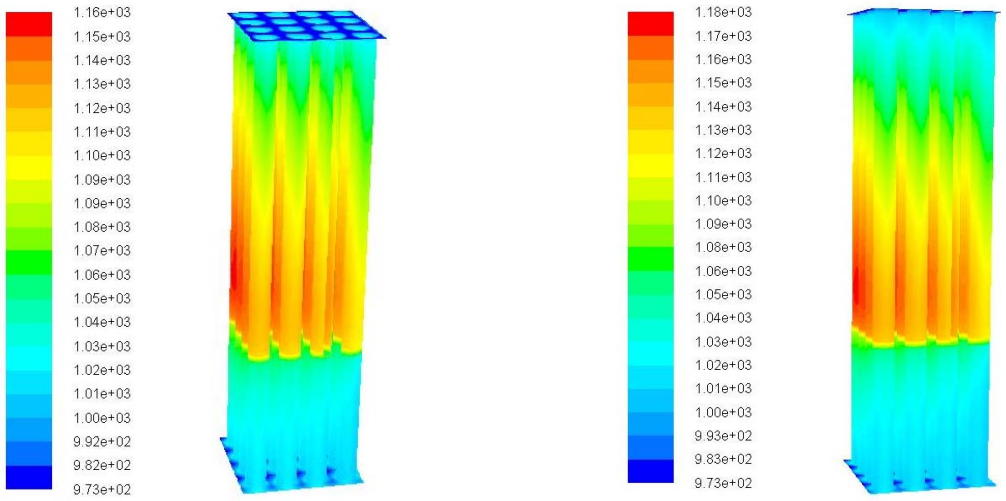

(a) (b)

Fig. 11. Temperature distributions of the fuel cell tubes at the air inlet velocity of 8.5 ms^{-1} with 7500 Wm^{-2} stack heat losses for two shape parameters: (a) a = 5 m^{-1} and (b) a = 10 m^{-1}

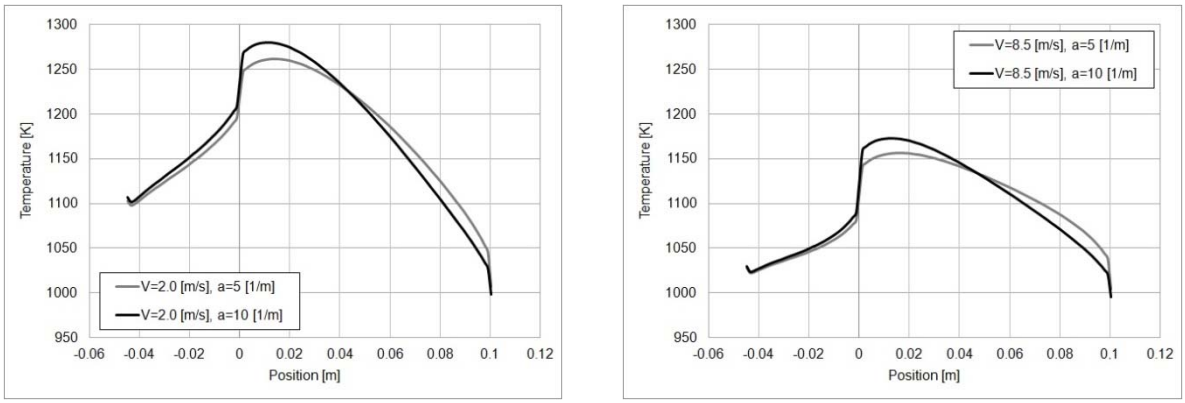

(a) (b)

Fig. 12. Temperature distributions along a middle fuel cell tube for SOFC linear heat flux with a = 5 and 10 m^{-1} for the air flow velocities of (a) 2.0 and (b) 8.5 ms^{-1}

4. CONCLUSIONS

A 3D comprehensive model was developed to simulate heat transfer of the microtubular Solid Oxide Fuel Cell stack and to estimate the influence of heat losses on the thermal conditions in the stack. Calculations were made for the fuel cell stack using two values of the cathode air velocity of 2.0 and 8.5 ms^{-1} and three values of the heat losses of 5, 10 and 50%. The results of steady – state simulation led to the following conclusions:

- until stack losses are up to 5 – 10% of the mSOFC reaction heat flux, the losses have a very low impact on the stack thermal conditions,
- the influence of the heat losses increases with decreasing air flow velocity,
- the heat losses increase the temperature gradients along the mSOFC stack,
- the area with the maximum temperature gradient values was at the boundary between the active part of the fuel cell tube and the inert one,
- the maximum difference between the temperature of the middle fuel cell tube and that of the peripheral one was about 50°C at the two air velocities studied and for 0, 5 and 10% of heat losses, while that difference at 50% of heat losses was about 80°C,
- electrochemically driven non-uniformities of the SOFC heat flux resulted in an increase of temperature gradients and the maximum temperature in the stack.

The presented CFD results seem to have enhanced the knowledge related to heat transfer and temperature distributions in the microtubular Solid Oxide Fuel Cell stack. Based on the CFD results, a proper selection of the inlet temperature and air flow rate in the fuel cell stack is possible, enabling to maintain the operating temperature below the maximum allowed and to obtain low enough temperature gradients, which may extend the fuel cell life time.

The research programme leading to these results received funding from the European Union's Seventh Framework Programme (FP7/2007-2013) for the Fuel Cells and Hydrogen Joint Technology Initiative under grant agreement no [278629]. Information contained in the paper reflects only view of the authors. The FCH JU and the Union are not liable for any use that may be made of the information contained therein. Acknowledgments are due to the partners of SUAV: E. de Wit, M. Walter, J. P. Brouwer of HyGear Fuel Cell Systems B.V., The Netherlands; M. Kendall, K. Kendall of Adelan Ltd., UK; T. Hargitai, F. Silversand, A. K. Jannasch, M. Lenberg, Ch. Karlsson of Catator AB,

Sweden; V. Antonucci, A.S. Arico, M. Ferraro of Consiglio Nazionale delle Ricerche, Italy; G. Schramm, M. Yadira, Narvaez-Clemente of EADS Deutschland GmbH, Germany; J. Price, T. Owen, M. Maynard of EADS UK Ltd.; E. Erdle of efceco, Germany; R. Steinberger - Wilckens, A. Dhir, B. Hari, T. Meadowcroft of The University of Birmingham, UK; E. Georges, J. Chapuis, J. M. Masenelli of SURVEY Copter, France.

The work was also financed from the Polish research funds awarded for the project No. W20317.PR/2011 of international cooperation within SUAV in years 2011-2014.

SYMBOLS

a	shape parameter of the heat flux profile, m^{-1}
c_p	average specific heat, $J \cdot kg^{-1} \cdot K^{-1}$
F_{kj}	view factor, -
g	acceleration due to gravity, $m^2 \cdot s^{-1}$
j	number of surface, -
k	number of surface, -
p	pressure, Pa
P_{el}	electric power density, $W \cdot cm^{-2}$
T	temperature, K
$\bar{u}$	velocity, $m \cdot s^{-1}$
q	heat flux, $W \cdot cm^{-2}$
$q_{in,\,k}$	energy flux incident on the surface from surrounding, $W \cdot cm^{-2}$
q_{max}	maximum value of heat flux, $W \cdot cm^{-2}$
q_{mean}	surface-averaged value of SOFC heat flux, $W \cdot cm^{-2}$
$q_{out,k}$	energy flux leaving the k^{th} surface, $W \cdot cm^{-2}$
z	axial coordinate of SOFC tube, m

Greek symbols

$\varepsilon_{cathode}$	cathode emissivity, -
ε_k	surface emissivity, -
λ	heat conductivity, $W \cdot m^{-1} \cdot K^{-1}$
μ	dynamic viscosity, Pa·s
ρ	density, $kg \cdot m^{-3}$
σ	Boltzmann constant, $eV \cdot K^{-1}$
η	electrical efficiency, %

REFERENCES

Akhtar N., Decent S.P., Kendall K., 2010. Numerical modelling of methane-powered microtubular single chamber solid oxide fuel cell. *J. Power Sources*, 195, 7796-7807. DOI: 10.1016/j.powesourc.2010.01.084.

Akhtar N., 2012. Microtubular, single-chamber solid oxide fuel cell (MT-SC-SOFC) stacks: Model development. *Chem. Eng. Res. Des*., 90, 814-824. DOI: 0.1016/j.cherd.2011/09/013.

Amiri S., Hayes R. E., Nandakumar K., Sarkar P., 2013. Modelling heat transfer for a tubular micro-solid oxide fuel cell with experimental validation. *J. Power Sources,* 233, 190-201. DOI: 10.1016/j.jpowsourc.2013.01.070.

Andersson M., Yuan J., Sunden B., 2012. SOFC modeling considering electrochemical reactions at the active three phase boundaries. *Intern. J. Heat Mass Transfer*, 55, 773-788. DOI: 10.1016/j.ijheatmasstransfer.2011.10.032.

Cui D., Cheng M., 2009. Numerical analysis of thermal and electrochemical phenomena for anode supported microtubular SOFC. *AIChE J*., 55, 3, 771-782. DOI: 10.1002/aic.11697.

Cui D., Liu L., Dong Y., Cheng M., 2007. Comparison of different current collecting modes of anode supported micro-tubular SOFC through mathematical modeling. *J. Power Sources*, 174, 246-254. DOI: 10.1016/j.powsourc.2007.08.094.

Doraswami U., Droushiotis N., Kelsall G.H., 2010. Modelling effects of current distributions on performance of micro-tubular hollow fibre solid oxide fuel cells. *Electrochim. Acta*, 55, 3766-3778. DOI: 10.1016/j.electa.2010.01.080.

Howe K., Thompson G.J., Kendal K., 2011. Micro-tubular solid oxide fuel cells and stacks. *J. Power Sources*, 196, 1677–1686. DOI: 10.1016/j.jpowsour.2010.09.043.

Howe K. S., Hanifi A. R., Kendall K., Zazulak M., Etsell T. H., Sarkar P., 2013. Performance of microtubular SOFCs with infiltrated electrodes under thermal cycling, International Journal of Hydrogen Energy, 38, 1058-1067. DOI: 10.1016/j.ijhydene.2012.10.098.

Huang B., Qi Y., Murshed A.K.M.M., 2013. *Dynamic modelling and predictive control in Solid Oxide Fuel Cells: First principle and data based approaches*. 1st edition, John Wiley & Sons, 8, 193-211.

Lee S.B., Lim T.H., Song R.H., Shin D.R., Dong S.K., 2008. Development of a 700 W anode-supported micro-tubular SOFC stack for APU applications. *Inter. J. Hydrogen Energy*, 33, 2330-2336. DOI: 10.1016/j.ijhydene.2008.02.034.

Lockett M., Simmons M.J.H., Kendall K., 2004. CFD to predict temperature profiles for scale up of microtubular SOFC stacks. *J. Power Sources,* 131, 243-246. DOI: 10.1016/j.powsour.2003.11.082.

Morata A., Meadowcroft A., Torell M.,Kendall K., Kendall M., Tarancon A., 2014. Characterization of microtubular Solid Oxide Fuel Cells for mobile application. *11th European SOFC & SOE Forum*, 1-4 July 2014, Lucerne, Switzerland.

Meier Ch., Hocker Th. Bieberle-Hutter A., Gauckler L., 2012. Analyzing a micro-solid oxide fuel cell system by global energy balances. *Int. J. Hydrogen Energy,* 37, 10318-10327. DOI: 10.1016/j.ijhydene.2012.04.009.

Milewski J., Świrski K., Santarelli M., Leone P., 2011. *Advanced methods of Solid Oxide Fuel Cell modeling*. Springer-Verlag London, 41-62. DOI: 10.1007/978-0-85729-262-9_3.

Received 01 November 2013
Received in revised form 04 April 2014
Accepted 23 May 2014